

Two-qubit controlled-PHASE Rydberg blockade gate protocol via off-resonant modulated driving within a single pulse

Yuan Sun,^{1,2,*} Peng Xu,^{3,4} and Ping-Xing Chen²

¹*Key Laboratory of Quantum Optics and Center of Cold Atom Physics,
Shanghai Institute of Optics and Fine Mechanics,
Chinese Academy of Sciences, Shanghai 201800, China*

²*Interdisciplinary Center for Quantum Information,
National University of Defense Technology, Changsha 410073, China*

³*State Key Laboratory of Magnetic Resonance and Atomic and Molecular Physics,
Wuhan Institute of Physics and Mathematics, Chinese Academy of Sciences
– Wuhan National Laboratory for Optoelectronics, Wuhan 430071, China*

⁴*Center for Cold Atom Physics, Chinese Academy of Sciences, Wuhan 430071, China*

Neutral atom array serves as an ideal platform to study the quantum logic gates, where intense efforts have been devoted to improve the two-qubit gate fidelity. We report our recent findings in constructing a different type of two-qubit controlled-PHASE quantum gate protocol with neutral atoms enabled by Rydberg blockade, which aims at both robustness and high-fidelity. It relies upon modulated driving pulse with specially tailored smooth waveform to gain appropriate phase accumulations for quantum gates. The major features include finishing gate operation within a single pulse, not necessarily requiring individual site addressing, not sensitive to the exact value of blockade shift while suppressing population leakage error and rotation error. We anticipate its fidelity to be reasonably high under realistic considerations for errors such as atomic motion, laser power fluctuation, power imbalance, spontaneous emission and so on. Moreover, we hope that such type of protocol may inspire future improvements in quantum gate designs for other categories of qubit platforms and new applications in other areas of quantum optimal control.

I. INTRODUCTION

Efficient, robust and high-fidelity two-qubit controlled-PHASE gate has become one of the central topics in the research frontier of quantum information with neutral atoms, which is not only important for quantum logic processing [1–3], but also crucial for quantum simulation [4] and quantum metrology [5, 6]. Rydberg blockade [7–9] emerges as one essential tool for this purpose, where the rapid progress in related studies over the past two decades, both theoretical and experimental, has already found many key advances in quantum information science and technology with neutral atoms [2, 3, 10–18]. One prominent feature of neutral atoms is that they serve as not only good candidates for qubit registers, but also good choices for quantum interface with light, where Rydberg blockade has been deemed as a critical element on both sides [14, 19–29].

Ever since the seminal paper of Ref. [30] which pioneered in the field of quantum computing with neutral atoms, many mechanisms of constructing two-qubit controlled-PHASE gate via Rydberg blockade have been studied extensively so far. Typically, a fast and robust gate mechanism requires relatively strong blockade shift. For those feasible gate protocols readily compatible with the currently mainstream atomic physics experimental platforms, it seems to us that they can be approximately divided into four categories. Category I. Rydberg blockade gate with the so-called π -gap- π pulse sequence, which

comes from the initial gate designs in Ref. [30]. It attracts persistent theoretical interests and serves as the current mainstream blueprint for serious experimental efforts, although it requires individual site addressing. Recent progress has suggested that the gate operation can be performed on the order of several hundred nanoseconds [31–34]. Nevertheless, gate fidelities reported from several labs are still at a little distance away from 99%, which may be partly due to several potential shortcomings embedded in this type of protocol, including a stringent requirement on ground-Rydberg coherence. Category II. Rydberg dressing, which was first conceived in the context of quantum gases [35]. The blockade effect can also be explored via Rydberg dressing of the ground state atoms [36, 37], which can in turn yield a two-qubit controlled-PHASE gate protocol [38, 39]. However, it usually needs a relatively long gate time which foreshadows gate fidelity due to the finite Rydberg level life time. Besides its role in the universal quantum computing, Rydberg dressing is suitable for implementing adiabatic quantum computation such as quantum annealing [40], and finds important applications in constructing multi-qubit quantum simulator [4, 41]. Category III. Rydberg anti-blockade gate [42, 43]. Such gate protocols usually requires the exact knowledge of the blockade shift [44], and are practically more sensitive to fluctuations of the relative motion between two atoms. Category IV. Protocols with simplified pulse sequence but more theoretical compromises, whose best achievable fidelity is less than ideal but relatively straightforward for experimental demonstration. For example, recently Ref. [45] discussed such a gate protocol with a single square pulse

* email: sunyuan17@nudt.edu.cn

driving ground-Rydberg transition. The major challenge for those protocols is to improve the highest theoretical fidelity limit to fit scalable purpose or fault-tolerant quantum computing.

Over the years, intense efforts have been devoted to analyzing performances of Rydberg blockade gate [8, 33, 34, 46, 47], where both the protocol's inherent physical limitations and technical imperfections have been taken into consideration. Very often, techniques of adiabatic passage [48, 49], including STIRAP [50, 51], are employed together with the π -gap- π [34] and Rydberg dressing [38] gate protocols. Tuning the Förster resonance with dc electric fields [52] or microwave have been also anticipated to facilitate gate performance. Nevertheless, experimental fidelities from those two-qubit gate mechanisms seem relatively less optimistic at this moment, despite the overall rapid progress in this field. Therefore, there exists strong demand for further explorations in gate protocols of potentially different recipes which may overcome known inconveniences in existing protocols.

In this article, we report our recent progress in theoretically devising and analyzing a Rydberg blockade type of two-qubit controlled-PHASE gate protocol for neutral atoms via Rydberg blockade, whose working principles rely upon atom-light interaction with a single off-resonant modulated laser pulse driving the ground-Rydberg transition. The modulation of the pulse waveform is engineered such that within the required fidelity, both the control and target atoms will return to original state no matter the blockade takes place or not, while gaining the correct phases as required by the two-qubit gate. Approximately speaking, this type of protocol combines the advantages of the π -gap- π gate and Rydberg dressing gates in a hybrid form, while avoiding shelving steady population on Rydberg state of control atom for a finite time gap during gate operation and gaining more robustness against noises. The rest of this article is organized as follows, first we present the basic mechanisms of our gate protocol, then we analyze and discuss the results, and finally we conclude the article. Relevant technical details, specifics of derivations and extra examples are included in the supplementary material.

II. BASIC MECHANISM

We start with the basic ingredients, where relevant atomic states of the atom-light interaction are shown in Fig. 1. The qubit basis states of the atoms may be represented by a pair of long-lived hyperfine ground clock states for typical alkali atoms, which can be manipulated by external microwave field or optical stimulated Raman transition [2, 9, 54]. Modulated laser pulses will be applied to drive the ground-Rydberg transitions of the control and target atoms. The consequences of the required operation can be abstracted into two aspects: the boomerang condition that the population re-

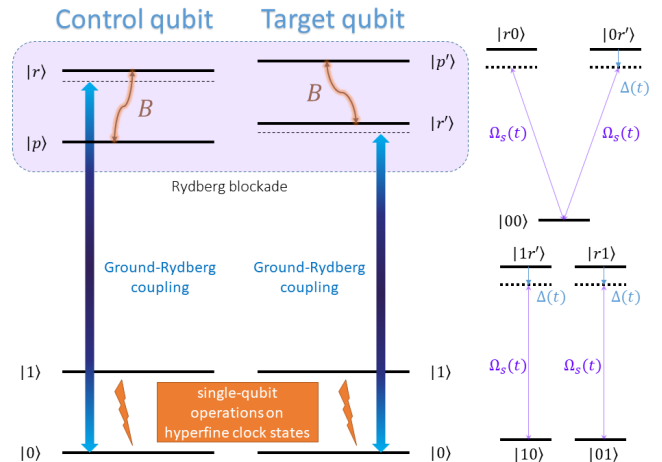


FIG. 1. Schematic of atomic structure for the Rydberg phase gate under investigation. On the left: the relevant atomic states including the Rydberg blockade between $|r\rangle$ and $|r'\rangle$, where the lasers are driving $|0\rangle \leftrightarrow |r\rangle$ on control atom and $|0\rangle \leftrightarrow |r'\rangle$ on target atom; on the right: under ideal blockade situation, the linkage pattern for states participating the ground-Rydberg transitions $|01\rangle, |10\rangle$ and $|00\rangle$. See Morris-Shore transform at Ref. [53] for a better explanation of comprehending linkage structures. State $|11\rangle$ does not participate the prescribed interactions and stays unchanged through the process. Rydberg states $|r\rangle$ and $|r'\rangle$ may be the same or different, depending on the choice of Förster resonance structure.

turns with unity probability and the antithesis condition that the accumulated phases achieve controlled-Z (C-Z) gate result. When combined with a local Hadamard gate on the target qubit atom ($\pi/2$ rotation for transition $|0\rangle \leftrightarrow |1\rangle$) before and after the controller-PHASE gate, this leads to the universal controlled-NOT gate [8, 9, 30]. If $|r\rangle, |r'\rangle$ are the same state, then individual atom addressing may not be mandatory and the experiment can be operated through one single laser. For simplicity, throughout this article the condition of symmetric driving will be presumed, namely both the qubit atoms will receive the same Rabi frequency and detuning in their effective ground-Rydberg transitions.

Assuming the presence of ideal Rydberg blockade such that double Rydberg excitation $|rr'\rangle$ is impossible. Define the state $|R\rangle = (|r0\rangle + |0r'\rangle)/\sqrt{2}$, there exist three types of couplings: $|10\rangle \leftrightarrow |1r\rangle, |01\rangle \leftrightarrow |r1\rangle$ with Rabi frequency Ω_s and $|00\rangle \leftrightarrow |R\rangle$ with Rabi frequency $\sqrt{2}\Omega_s$, as can be seen in the linkage structure of Fig. 1. The goal is to find an atom-light interaction process such that the induced changes in the wave functions conforms to the two-qubit phase gate after the interaction is over. More specifically, let (C_0, C_r) denote the wave function for the ground-Rydberg transition of $|10\rangle$ or $|01\rangle$, and let (X_0, X_R) denote the wave function for the ground-Rydberg transition of $|00\rangle$. The problem reduces to determine proper and feasible Ω_s, Δ for the time evolution:

$$i \frac{d}{dt} \begin{bmatrix} C_0 \\ C_r \end{bmatrix} = \begin{bmatrix} 0 & \frac{1}{2}\Omega_s \\ \frac{1}{2}\Omega_s^* & \Delta \end{bmatrix} \cdot \begin{bmatrix} C_0 \\ C_r \end{bmatrix}; \quad (1a)$$

$$i \frac{d}{dt} \begin{bmatrix} X_0 \\ X_R \end{bmatrix} = \begin{bmatrix} 0 & \frac{\sqrt{2}}{2}\Omega_s \\ \frac{\sqrt{2}}{2}\Omega_s^* & \Delta \end{bmatrix} \cdot \begin{bmatrix} X_0 \\ X_R \end{bmatrix}. \quad (1b)$$

It turns out, appropriate solutions may be obtained, where the practical task becomes to find them out and examine their properties. Our tactics involve careful refining efforts for modulations from heuristic approaches. More specifically, first we design waveforms under assumption of perfect adiabatic time evolution process in Eq. (1), and then perform optimizations to suppress the non-adiabaticity effects [55], where numerical tools serves an essential role in this process.

Except for technical noises, we think that two main types of intrinsic errors exist: the population leakage error due to spontaneous emission of Rydberg levels during interaction, and the rotation error due to the less than ideal Rydberg blockade with double Rydberg excitation. Nevertheless, with properly tailored smooth pulses, the mechanism of adiabatically tracking two-atom dark state gets implicitly triggered under the presence of dipole-dipole exchange interaction $|rr'\rangle \leftrightarrow |pp'\rangle$ [55]. Therefore, the rotation error will be suppressed as we may observe in later discussions.

III. RESULTS AND DISCUSSIONS

For $|01\rangle$ and $|10\rangle$, the dynamics amounts to nothing more than a two-level system made from ground-Rydberg transition with time-dependent Rabi frequency $\Omega_s(t)$ and detuning $\Delta(t)$. On the other hand, for $|00\rangle$, its dynamics actually probes the Rydberg dipole-dipole interaction, whose linkage pattern may be summarized as $|00\rangle \leftrightarrow |R\rangle \leftrightarrow |rr'\rangle \leftrightarrow |pp'\rangle$. In order to quantitatively describe the Förster resonance structure of $|rr'\rangle \leftrightarrow |pp'\rangle$, we assume that the coupling strength is B and the small Förster energy penalty term is δ_p for $|pp'\rangle$. The interaction Hamiltonian is then:

$$H_I/\hbar = \frac{\sqrt{2}}{2}\Omega_s|R\rangle\langle 00| + \frac{\sqrt{2}}{2}\Omega_s|rr'\rangle\langle R| + \text{H.c.} + \Delta|R\rangle\langle R| + 2\Delta|rr'\rangle\langle rr'|, \quad (2)$$

where we have already included rotating wave approximation. We include Rydberg blockade as:

$$H_F/\hbar = B|pp'\rangle\langle rr'| + \text{H.c.} + \delta_p|pp'\rangle\langle pp'|. \quad (3)$$

Following the prescribed recipes, we have obtained two categories of waveforms that yield two-qubit phase gate with satisfying performances. One of them requires amplitude and frequency modulations simultaneously, while the other one only requires amplitude modulation with a constant detuning.

For the waveform of both amplitude and frequency

modulations, we make the designing goal a little more strict than necessary, such that the aim is for a standard C-Z gate where the population returns with a phase change of 0 for $|01\rangle$ and $|10\rangle$ and a phase change of π for $|00\rangle$ after interaction. Beginning with heuristic approaches [55], we find out the sinusoidal modulations fit well for this category after the refining work on the time evolution details. In particular, we have selected a set of waveforms described in the following:

$$\Omega_s(t) = \Omega_0 + \Omega_1 \cos(2\pi t/T_g) + \Omega_2 \sin(\pi t/T_g); \quad (4a)$$

$$\Delta(t) = \Delta_0 + \Delta_1 \cos(2\pi t/T_g) + \Delta_2 \sin(\pi t/T_g). \quad (4b)$$

Via optimizations under the prescribed constraints, we have identified a set of values as: $\Omega_0 = 2.564, \Omega_1 = 0.950, \Omega_2 = 0.116, \Delta_0 = 1.004, \Delta_1 = -1.093, \Delta_2 = -0.002$; all coefficient units are MHz, and the gate time

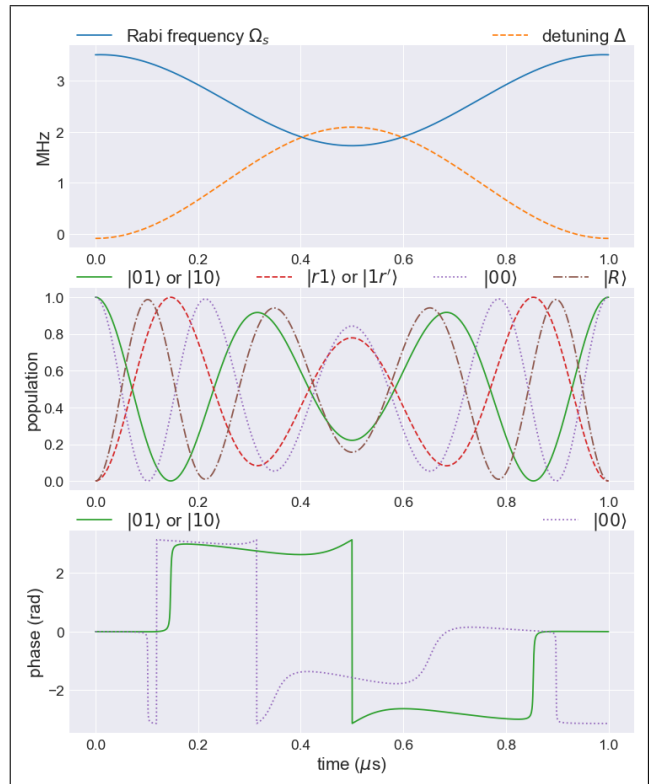


FIG. 2. Numerical simulation of the time evolution. Modulation is configured as stated in the text, while $B = 2\pi \times 500$ MHz, $\delta_p = 2\pi \times -3$ MHz. The first graph shows the waveform, the second graph shows the population on different atomic states, while the last graph shows the phase accumulation of the atomic wave function during the process. The purpose is C-Z gate, and the fidelity of this example is 0.99997. To evaluate fidelity, we first numerically calculate the outcome wave functions from the time evolution. Then, with respect to the four basis states $|00\rangle, |01\rangle, |10\rangle, |11\rangle$, we acquire the 4 by 4 transform matrix U representing our gate operation. Then the fidelity may be calculated as $F = (\text{Tr}(MM^\dagger) + |\text{Tr}(M)|^2)/20$, with $M = U_{C-Z}^\dagger U$ with U_{C-Z} being the transform matrix of an ideal C-Z gate.

T_g is set as $1 \mu\text{s}$. To demonstrate the detailed dynamics of the system with respect to the Hamiltonian of Eq. (2), we present the numerical simulation results in Fig. 2 without considerations for spontaneous emissions of Rydberg levels and technical noises. The modulation does not involve unreasonable high frequency components, and the atomic wave function does not go through ‘sudden’ change during the course of gate operation. We have intentionally chosen a symmetric waveform, which simplifies the calculation process but is not mandatory. For dynamics associated with $|00\rangle$, although the situation is more complicated than the two-level system considered in Eq. (1), a clear signature is that the population returns almost ideally with no significant portion trapped in the Rydberg level, thanks to the adiabatic dark state driving mechanism in Rydberg blockade effect [55].

For the other category of only amplitude modulation, it is preferred that the pulse starts and ends at zero intensity. Among several candidate waveforms, we are particularly interested in the ones of relatively less complexities, such as:

$$\Omega_s(t) = \sum_{\nu=1}^4 \beta_{\nu} (b_{\nu,n}(t/T_g) + b_{n-\nu,n}(t/T_g)); \quad (5a)$$

$$\Delta(t) = \Delta_0 \equiv \text{constant}; \quad (5b)$$

where $b_{\nu,n}$ is the ν th Bernstein basis polynomials of degree n [55], we set $n = 8$ and we again intentionally configure a symmetric waveform. The result we pursue is in fact a controlled-PHASE gate, and local sing-qubit phase rotation is required if we want conversion into C-Z gate. The associated phase constraint is:

$$\phi_{11} = \pm\pi - \phi_{00} + \phi_{01} + \phi_{10}, \quad (6)$$

where $\phi_{01} + \phi_{10} - \phi_{00} = \pm\pi$ if $\phi_{11} = 0$.

Next, we seek a set of values leading to appropriate phase gate performance. After optimization efforts, for gate time T_g is set as $1 \mu\text{s}$, we have reached a set of satisfying parameters, $\beta_1 = 1.419, \beta_2 = 0, \beta_3 = 5.076, \beta_4 = 13.425, \Delta_0 = -3.512$; all coefficient units are MHz. The corresponding numerical simulation is shown in Fig. 3. The singly-excited Rydberg state $|R\rangle$ is not heavily populated throughout the interaction process, which does not share the same behavior as the obvious feature of quantum Rabi oscillation in Fig. 2. This is due to the difference in the underlying physics mechanisms between those two cases, where Fig. 2 shares similarities with a typical quantum Rabi oscillation and Fig. 3 shares similarities with adiabatic rapid passage, and this may be observed from their paths on Bloch sphere. Nevertheless, both approaches are suitable choices for the purpose of two-qubit phase gate.

We observe that the mechanism of adiabatically tracking the two-atom dark state also plays an essential role here [55]. The amplitude modulation does not only introduce the correct change in atomic wave functions for a phase gate with respect to Eq. (1) and Eq. (6), but also

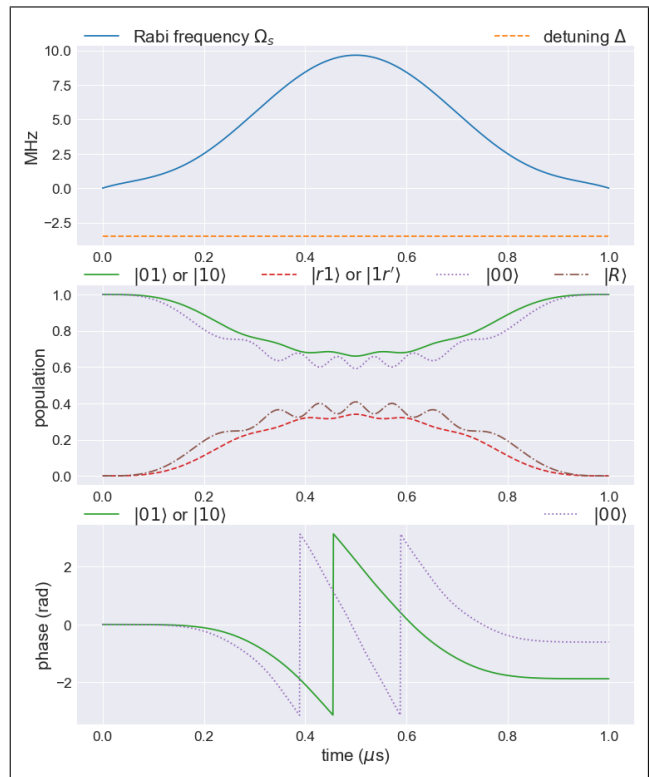


FIG. 3. Numerical simulation of the time evolution with amplitude modulated pulse. The waveform is set as Eq. (5), while $B = 2\pi \times 500$ MHz, $\delta_p = 2\pi \times -3$ MHz. The first graph shows the waveform, the second graph shows the population on different atomic states, while the last graph shows the phase accumulation of the atomic wave function during the process. After appropriate local phase rotations to adjust it to a standard C-Z gate, its gate error \mathcal{E} is way below 1×10^{-5} , defined as $\mathcal{E} = 1 - F$. Spontaneous emissions of Rydberg levels and technical noises are not considered here.

helps to suppress the rotational error. In other words, major limitations on the attainable fidelity are anticipated to mostly come from spontaneous emissions, modulation imperfections and technical noises.

Furthermore, we need to estimate the influences of the major intrinsic error source of spontaneous emission. We carry out numerical evaluations by resorting to quantum jump approach [56, 57], also known as Monte-Carlo wave function (MCWF). The result is shown in Fig. 4, where we compute gate error as a function of the Rydberg decay rates. We deduce that in principle the Rydberg levels’ spontaneous emission is the dominating theoretical limiting factor in achieving high-fidelity, provided the Rydberg blockade shift is strong enough.

We have also investigated the influence to gate performance from realistic imperfections commonly encountered in experiments, including amplitude fluctuations in the laser pulse, residual thermal motion of the cold atoms and laser power imbalance at the two qubit sites [55]. We observe that the gate protocol is robust against these types of disturbance as long as they are kept at a

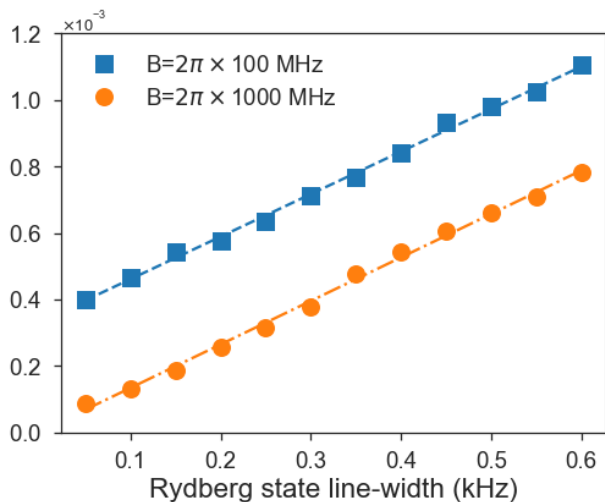


FIG. 4. Numerical simulation for gate error \mathcal{E} with gate time set as $1 \mu\text{s}$ and the waveform set as Fig. 3. Each data point is extracted from 200,000 MCWF trajectories. Two values of B are considered, all with $\delta_p = 2\pi \times -3$ MHz. For simplicity, the spontaneous decay rates of all Rydberg states are taken as the same. Fittings to a straight lines indicates that the linear relation holds well between Rydberg decay rate and gate error, for the parameter range we are interested in.

reasonably low level. When considering the off-resonant driving for the ground-Rydberg transition, we've concentrated on the few states that are directly involved in the mechanism. Realistically, the situation is more complicated due to the atom's many other levels, which may introduce various sources of extra ac Stark shifts and decoherences [33, 46].

Several major characteristics are worth mentioning here. It may work without individual addressing on the qubit atoms. No microwave is required to drive the Rydberg-Rydberg transitions and henceforth it saves trouble of the complicated microwave electronic equipment and antennas. It does not require the exact knowledge of the magnitude of the Rydberg blockade shift. Its working condition does not involve far off-resonance detuning as that of Rydberg dressing and therefore the gate may be designed to fast operation below $1 \mu\text{s}$ with respect to realistic experimental apparatus parameters. Carrying out two-qubit entangling gate within a single continuous shaped driving pulse has already become a common practice in other platforms such as the super-

conducting qubit [58], and we think it is beneficial to design a counterpart for neutral atom platform.

IV. CONCLUSION AND OUTLOOK

We have systematically presented our recent results in designing two-qubit controlled-PHASE Rydberg blockade gate protocol for neutral atoms via off-resonant modulated driving within a single pulse. In principle, the same guidelines may be extended to help construct a generic three-qubit gate such as Toffoli gate.

On the other hand, we believe that the result is not unique and a full characterization of accessible solutions remains an open problem. We are also looking forward to a few other future refinements, including the search for a faster gate operation, further suppression of population leakage, stronger robustness against environmental noises, and more user-friendly parameter setting. Error correction mechanism [59] for our gate protocol is also part of the long term goal.

For applications with readily available hardware in immediate future [2, 3], we expect that $\gtrsim 99\%$ fidelity may be obtained for two-qubit gate in 1D, 2D or 3D atomic arrays with a gate time less than $1 \mu\text{s}$. Our faith with the Rydberg blockade gate is that high-fidelity ground-Rydberg Rabi oscillation shall be directly translated into high-fidelity controlled-PHASE gate. We also anticipate that our work will help the endeavors for the ensemble qubit approach [20, 60] and the Rydberg-mediated atom-photon controlled-PHASE gate [23, 24, 26, 28].

ACKNOWLEDGMENTS

The authors gratefully acknowledge the funding support from the National Key R&D Program of China (under contract Grant No. 2016YFA0301504 and No. 2016YFA0302800). The authors also acknowledge the hospitality of Key Laboratory of Quantum Optics and Center of Cold Atom Physics, Shanghai Institute of Optics and Fine Mechanics. The authors gratefully thank the help from Professor Liang Liu, Professor Mingsheng Zhan and Professor Mark Saffman who essentially make this work possible. The authors also thank Professor Xiaodong He, Professor Dongsheng Ding and Professor Tian Xia for enlightening discussions.

-
- [1] L. Isenhower, E. Urban, X. L. Zhang, A. T. Gill, T. Henage, T. A. Johnson, T. G. Walker, and M. Saffman, *Phys. Rev. Lett.* **104**, 010503 (2010).
 [2] K. M. Maller, M. T. Lichtman, T. Xia, Y. Sun, M. J. Piotrowicz, A. W. Carr, L. Isenhower, and M. Saffman, *Phys. Rev. A* **92**, 022336 (2015).
 [3] Y. Zeng, P. Xu, X. He, Y. Liu, M. Liu, J. Wang, D. J.

- Papoular, G. V. Shlyapnikov, and M. Zhan, *Phys. Rev. Lett.* **119**, 160502 (2017).
 [4] H. Bernien, S. Schwartz, A. Keesling, H. Levine, A. Omran, H. Pichler, S. Choi, A. S. Zibrov, M. Endres, M. Greiner, V. Vuletić, and M. D. Lukin, *Nature* **551**, 579 (2017).
 [5] V. Giovannetti, S. Lloyd, and L. Maccone, *Nature Pho-*

- tonics **5**, 222 (2011).
- [6] C. L. Degen, F. Reinhard, and P. Cappellaro, *Rev. Mod. Phys.* **89**, 035002 (2017).
- [7] E. Urban, T. A. Johnson, T. Henage, L. Isenhower, D. D. Yavuz, T. G. Walker, and M. Saffman, *Nature Physics* **5**, 110 (2009).
- [8] M. Saffman, T. G. Walker, and K. Mølmer, *Rev. Mod. Phys.* **82**, 2313 (2010).
- [9] M. Saffman, *Journal of Physics B: Atomic, Molecular and Optical Physics* **49**, 202001 (2016).
- [10] M. Saffman and T. G. Walker, *Phys. Rev. A* **66**, 065403 (2002).
- [11] E. Brion, K. Mølmer, and M. Saffman, *Phys. Rev. Lett.* **99**, 260501 (2007).
- [12] J. Honer, R. Löw, H. Weimer, T. Pfau, and H. P. Büchler, *Phys. Rev. Lett.* **107**, 093601 (2011).
- [13] A. V. Gorshkov, J. Otterbach, M. Fleischhauer, T. Pohl, and M. D. Lukin, *Phys. Rev. Lett.* **107**, 133602 (2011).
- [14] V. Parigi, E. Bimbard, J. Stanojevic, A. J. Hilliard, F. Nogrette, R. Tualle-Brouri, A. Ourjoumtsev, and P. Grangier, *Phys. Rev. Lett.* **109**, 233602 (2012).
- [15] Y. O. Dudin and A. Kuzmich, *Science* **336**, 887 (2012).
- [16] D. Maxwell, D. J. Szwer, D. Paredes-Barato, H. Busche, J. D. Pritchard, A. Gauguier, K. J. Weatherill, M. P. A. Jones, and C. S. Adams, *Phys. Rev. Lett.* **110**, 103001 (2013).
- [17] H. Gorniaczyk, C. Tresp, J. Schmidt, H. Fedder, and S. Hofferberth, *Phys. Rev. Lett.* **113**, 053601 (2014).
- [18] C. Tresp, C. Zimmer, I. Mirgorodskiy, H. Gorniaczyk, A. Paris-Mandoki, and S. Hofferberth, *Phys. Rev. Lett.* **117**, 223001 (2016).
- [19] D. Paredes-Barato and C. S. Adams, *Phys. Rev. Lett.* **112**, 040501 (2014).
- [20] M. Ebert, M. Kwon, T. G. Walker, and M. Saffman, *Phys. Rev. Lett.* **115**, 093601 (2015).
- [21] O. Lahad and O. Firstenberg, *Phys. Rev. Lett.* **119**, 113601 (2017).
- [22] M. Khazali, K. Heshami, and C. Simon, *Phys. Rev. A* **91**, 030301 (2015).
- [23] Y. M. Hao, G. W. Lin, K. Xia, X. M. Lin, Y. P. Niu, and S. Q. Gong, *Sci. Rep.* **5**, 10005 (2015).
- [24] S. Das, A. Grankin, I. Iakoupov, E. Brion, J. Borregaard, R. Boddeda, I. Usmani, A. Ourjoumtsev, P. Grangier, and A. S. Sørensen, *Phys. Rev. A* **93**, 040303 (2016).
- [25] J. Ningyuan, A. Georgakopoulos, A. Ryou, N. Schine, A. Sommer, and J. Simon, *Phys. Rev. A* **93**, 041802 (2016).
- [26] A. C. J. Wade, M. Mattioli, and K. Mølmer, *Phys. Rev. A* **94**, 053830 (2016).
- [27] J. Lee, M. J. Martin, Y.-Y. Jau, T. Keating, I. H. Deutsch, and G. W. Biedermann, *Phys. Rev. A* **95**, 041801 (2017).
- [28] Y. Sun and P.-X. Chen, *Optica* **5**, 1492 (2018).
- [29] D. Tiarks, S. Schmidt-Eberle, T. Stolz, G. Rempe, and S. Duerr, *NATURE PHYSICS* **15**, 124 (2019).
- [30] D. Jaksch, J. I. Cirac, P. Zoller, S. L. Rolston, R. Côté, and M. D. Lukin, *Phys. Rev. Lett.* **85**, 2208 (2000).
- [31] T. Xia, X. L. Zhang, and M. Saffman, *Phys. Rev. A* **88**, 062337 (2013).
- [32] I. I. Beterov and M. Saffman, *Phys. Rev. A* **92**, 042710 (2015).
- [33] L. S. Theis, F. Motzoi, F. K. Wilhelm, and M. Saffman, *Phys. Rev. A* **94**, 032306 (2016).
- [34] D. Petrosyan, F. Motzoi, M. Saffman, and K. Mølmer, *Phys. Rev. A* **96**, 042306 (2017).
- [35] L. Santos, G. V. Shlyapnikov, P. Zoller, and M. Lewenstein, *Phys. Rev. Lett.* **85**, 1791 (2000).
- [36] I. Bouchoule and K. Mølmer, *Phys. Rev. A* **65**, 041803 (2002).
- [37] J. E. Johnson and S. L. Rolston, *Phys. Rev. A* **82**, 033412 (2010).
- [38] T. Keating, R. L. Cook, A. M. Hankin, Y.-Y. Jau, G. W. Biedermann, and I. H. Deutsch, *Phys. Rev. A* **91**, 012337 (2015).
- [39] Y.-Y. Jau, A. M. Hankin, T. Keating, I. H. Deutsch, and G. W. Biedermann, *Nature Physics* **12**, 71 (2015).
- [40] T. Keating, K. Goyal, Y.-Y. Jau, G. W. Biedermann, A. J. Landahl, and I. H. Deutsch, *Phys. Rev. A* **87**, 052314 (2013).
- [41] J. Zeiher, R. van Bijnen, P. Schau, S. Hild, J.-y. Choi, T. Pohl, I. Bloch, and C. Gross, *Nature Physics* **12**, 1095 (2016).
- [42] C. Ates, T. Pohl, T. Pattard, and J. M. Rost, *Phys. Rev. Lett.* **98**, 023002 (2007).
- [43] A. W. Carr and M. Saffman, *Phys. Rev. Lett.* **111**, 033607 (2013).
- [44] X.-F. Shi, *Phys. Rev. Applied* **7**, 064017 (2017).
- [45] R. Han, H. K. Ng, and B.-G. Englert, *EPL (Europhysics Letters)* **113**, 40001 (2016).
- [46] M. Saffman and T. G. Walker, *Phys. Rev. A* **72**, 022347 (2005).
- [47] T. G. Walker and M. Saffman, *Phys. Rev. A* **77**, 032723 (2008).
- [48] I. I. Beterov, M. Saffman, E. A. Yakshina, D. B. Tretyakov, V. M. Entin, S. Bergamini, E. A. Kuznetsova, and I. I. Ryabtsev, *Phys. Rev. A* **94**, 062307 (2016).
- [49] I. I. Beterov, G. N. Hamzina, E. A. Yakshina, D. B. Tretyakov, V. M. Entin, and I. I. Ryabtsev, *Phys. Rev. A* **97**, 032701 (2018).
- [50] D. D. B. Rao and K. Mølmer, *Phys. Rev. A* **89**, 030301 (2014).
- [51] Y. Sun and H. Metcalf, *Phys. Rev. A* **90**, 033408 (2014).
- [52] S. Ravets, H. Labuhn, D. Barredo, L. Bguin, T. Lahaye, and A. Browaeys, *Nature Physics* **10**, 914 (2014).
- [53] J. R. Morris and B. W. Shore, *Phys. Rev. A* **27**, 906 (1983).
- [54] T. Xia, M. Lichtman, K. Maller, A. W. Carr, M. J. Piotrowicz, L. Isenhower, and M. Saffman, *Phys. Rev. Lett.* **114**, 100503 (2015).
- [55] See Supplemental Material at URL for more underlying details..
- [56] J. Dalibard, Y. Castin, and K. Mølmer, *Phys. Rev. Lett.* **68**, 580 (1992).
- [57] M. B. Plenio and P. L. Knight, *Rev. Mod. Phys.* **70**, 101 (1998).
- [58] J. M. Chow, A. D. Córcoles, J. M. Gambetta, C. Rigetti, B. R. Johnson, J. A. Smolin, J. R. Rozen, G. A. Keefe, M. B. Rothwell, M. B. Ketchen, and M. Steffen, *Phys. Rev. Lett.* **107**, 080502 (2011).
- [59] D. Crow, R. Joynt, and M. Saffman, *Phys. Rev. Lett.* **117**, 130503 (2016).
- [60] M. Kwon, M. F. Ebert, T. G. Walker, and M. Saffman, *Phys. Rev. Lett.* **119**, 180504 (2017).

Supplemental Material:
Two-qubit controlled-PHASE Rydberg blockade gate protocol via off-resonant modulated driving within a single pulse

Yuan Sun,^{1,2,*} Peng Xu,^{3,4} and Ping-Xing Chen²

¹*Key Laboratory of Quantum Optics and Center of Cold Atom Physics,
Shanghai Institute of Optics and Fine Mechanics,
Chinese Academy of Sciences, Shanghai 201800, China*

²*Interdisciplinary Center for Quantum Information,
National University of Defense Technology, Changsha 410073, China*

³*State Key Laboratory of Magnetic Resonance and Atomic and Molecular Physics,
Wuhan Institute of Physics and Mathematics, Chinese Academy of Sciences*

- Wuhan National Laboratory for Optoelectronics, Wuhan 430071, China

⁴*Center for Cold Atom Physics, Chinese Academy of Sciences, Wuhan 430071, China*

(Dated: October 18, 2019)

* email: sunyuan17@nudt.edu.cn

This supplementary material is organized as the following. (I) The optimization procedure to compute the appropriate waveform. (II) More details about the two-atom dark state adiabatic driving mechanism. (III) Derivations about the handling of phase modulation. (IV) More information on the performance of the gate, including when it is subject to cold atom's residual thermal motion. (V) Sample calculation of 250 ns phase gate. (VI) Asymmetric driving process due to systematic in-accuracy.

I. PROCEDURE TO CALCULATE WAVEFORMS

In this section we discuss more details of the tactics to retrieve the appropriate waveforms to arrive at appropriate C-Z gate operation.

We start with the heuristic approach which serves as the precursor for our formal treatment under the framework of off-resonant modulated driving. It comes from a very elementary observation on the time evolution with respect to the two-level atom dressed states, when the atom is driven by modulated optical pulse. Namely, while neglecting non-adiabaticity, what the time evolution brings about can be recognized as phase accumulations on dressed states. Therefore, as long as the dressed states take the same form at the beginning and end, this heuristic approach will simply regard the effect caused by the atom-light interaction as a phase change. More specifically, for given Rabi frequency Ω_a and detuning δ_a , the interaction Hamiltonian matrix in the rotating wave frame, the dressed states energies, and the corresponding dressed states expressions are as the following:

$$\frac{1}{2} \begin{bmatrix} 0 & \Omega_a \\ \Omega_a^* & 2\delta_a \end{bmatrix}, \lambda_{+,-} = \frac{1}{2}\delta_a \pm \frac{1}{2}\sqrt{|\Omega_a|^2 + \delta_a^2}, \lambda_+ \sim \begin{bmatrix} \sin\theta e^{-i\varphi} \\ \cos\theta \end{bmatrix}, \lambda_- \sim \begin{bmatrix} \cos\theta e^{-i\varphi} \\ -\sin\theta \end{bmatrix}. \quad (1)$$

where $\hbar\lambda_{+,-}$ are the dress states' energies, or the so-called adiabatic energies; $\tan(2\theta) \equiv |\Omega_a|/\delta_a$ with $0 \leq \theta \leq \pi$ and $\varphi = \arg(\Omega_a)$. More details can be found at standard atomic physics textbooks.

Therefore, under this very intuitive observation, in order to simultaneously meet the requirement of returning full population to initial state and acquiring a proper phase change, I would like to impose two straightforward conditions: (1) $\Omega_a(t)$ takes the same value at the beginning and ending moments, and so is $\delta_a(t)$; (2) two dressed states accumulate the same phase under the adiabatic assumption $\Phi_d(\Omega_a, \delta_a) = \int \lambda_+(\Omega_a, \delta_a)dt = \int \lambda_-(\Omega_a, \delta_a)dt + 2N\pi$, $N = 1, 2, 3 \dots$, and the accumulated phase Φ_d will correspond to gate protocol's demands.

In the above formalism, the Rabi frequency Ω_a corresponds to the case of $|10\rangle \leftrightarrow |1r\rangle$, $|01\rangle \leftrightarrow |r1\rangle$, while the Rabi frequency $\sqrt{2}\Omega_a$ corresponds to the case of $|00\rangle \leftrightarrow (|r0\rangle + |0r'\rangle)/\sqrt{2}$ assuming perfect Rydberg blockade. With all these understandings, in order to meet the requirement of C-Z gate, one of the simplest forms of the condition imposed by this heuristic approach may be expressed as:

$$\Phi_d(\Omega_a, \delta_a) = 3\pi, \Phi_d(\sqrt{2}\Omega_a, \delta_a) = 4\pi. \quad (2)$$

When the smooth waveforms of Ω_a, δ_a are described by a set of discrete parameters $x_1, x_2, x_3 \dots$, the constraint of Eq. (2) turns into a set of equations which may be solved numerically. Nevertheless, due to the existence of non-adiabaticity, the waveforms computed by this heuristic approach do not yield the desired high-fidelity gate performance.

However, the basic principle behind the heuristic approach is appealing, where the ultimate goal is to construct a C-Z gate via a single modulated pulse with specially tailored smooth waveform to gain appropriate phase accumulations. Main advantages of this basic principle include avoiding depositing full population at Rydberg state for a finite gap time, avoiding Ramsey type pulse sequence which may put stringent requirement on ground-Rydberg T_2^* coherence time, while suppressing population leakage error and rotation error. The hope is to try overcoming the hurdles by resorting to helpful ideas of adiabatic rapid passage and numerical optimization methods, and this is exactly what we do next for the main purpose of this research effort.

Since we want to employ the tool of numerical methods, this naturally implies that the essentially continuous waveforms need to be represented by a set of discrete parameters such that they may be handled. And therefore we need to carry out a procedure of 'continuous to discrete', for which purpose the Fourier series and Bernstein polynomials float as ideal choices. From mathematical point of view, expansion of Fourier series or Bernstein polynomials form a complete basis for non-pathological functions defined on a finite time interval. Yet on practical account only a limited amount of terms in the expansion will be enough to compute a reasonable waveform for the purpose of gate protocol.

More specifically, we'd like to demonstrate more details here about the process of constructing waveforms for high fidelity gate protocol via resorting to Bernstein polynomials. A Bernstein polynomial is formed from the linear combination of Bernstein basis polynomials, and it becomes the building block of Bézier curves which is important in

modern computer graphics.

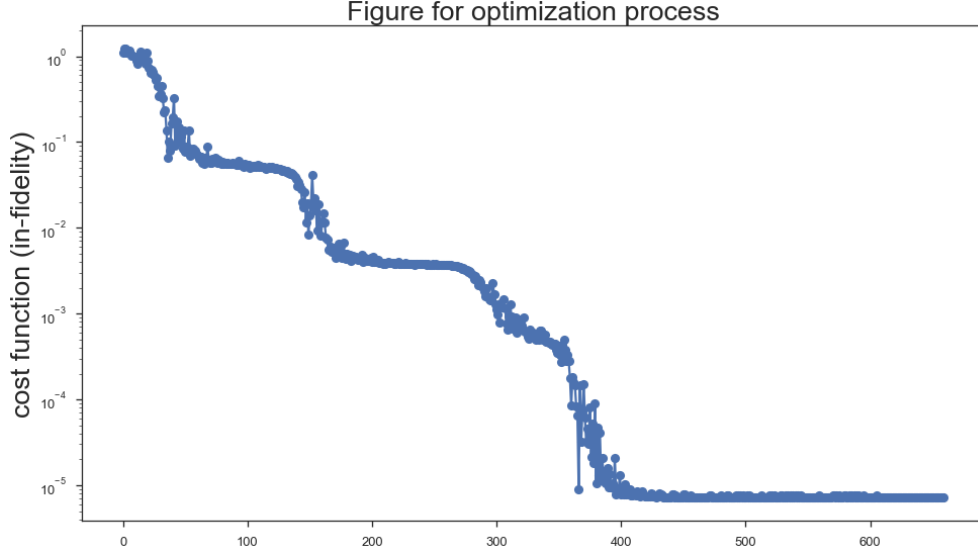


FIG. 1: A typical example of the waveform calculation process, via down-hill simplex numerical optimization method. Horizontal axis represents the index of iterations, while the vertical axis is for the value of cost function in log scale. As the general form of Eq. (5), the amplitude waveform is chosen as $\sum_{\nu=1}^4 \beta_{\nu} (b_{\nu,n}(t/T_g) + b_{n-\nu,n}(t/T_g))$ where we fix $n = 8$, and therefore the waveform is symmetric. The optimization process does not consume too much computation resource and converges quickly. The initial values are set as $\beta_1 = 1, \beta_2 = 2, \beta_3 = 10, \beta_4 = 6, \Delta_0 = -1$ while the calculated result is $\beta_1 = 1.129, \beta_2 = 0, \beta_3 = 4.801, \beta_4 = 15.038, \Delta_0 = -4.019$; all coefficient units are MHz. This example is for the amplitude-only modulation waveform.

For an integer n , the $n + 1$ Bernstein basis polynomials of degree n is defined on interval $[0, 1]$ as the following:

$$b_{\nu,n}(x) = \binom{n}{\nu} x^{\nu} (1-x)^{n-\nu}, \nu = 0, \dots, n; \quad (3)$$

where $\binom{n}{\nu} = \frac{n!}{(n-\nu)!\nu!}$ is the binomial coefficient. Then, a Bernstein polynomial may be expressed in terms of the basis polynomials as the following form:

$$B_n(x) = \sum_{\nu=0}^n \beta_{\nu} b_{\nu,n}(x), \quad (4)$$

where β_{ν} 's are real-value coefficients.

On practical account for experimental implementation, it is natural to hope for the amplitude of modulated waveform to start and end at zero, in order to avoid the sharp edge of sudden switching. One convenient feature of is that for $\nu \neq 0, n$, the value of $b_{\nu,n}(x)$ at the end points $0, 1$ is exactly zero. Therefore, it is convenient to aim for a truncated form of liner combinations as $B_n(x) = \sum_{\nu=1}^{n-1} \beta_{\nu} b_{\nu,n}(x)$ with respect to degree n , for the purpose of off-resonant driving with only amplitude modulation. That is, the candidate laser waveform may be expressed as:

$$\Omega_s(t) = \sum_{\nu=1}^{n-1} \beta_{\nu} b_{\nu,n}(t/T_g); \Delta(t) = \Delta_0 \equiv \text{constant}; \quad (5)$$

where the gate process is defined on time interval $[0, T_g]$.

Starting from Eq. (5), the task turns into finding a set of values β_{ν} that will yield adequate fidelity with respect to the C-Z gate requirement. Instead of an analytic method, we decide to resort to numerical optimization algorithms. And later on it turns out that the down-hill simplex method, also known as Nelder-Mead algorithm, performs particularly

well for our purpose. The cost function is chosen naturally as the in-fidelity $1 - F$ evaluated at the end time $t = T_g$ for the two-atom system. Meanwhile, during the optimization process, we keep the positiveness $\Omega_s(t) > 0$ all the time since if negative value of $\Omega_s(t)$ occurs on $t \in [0, T_g]$ it means a sudden phase change of the optical field, which is a pathological situation. The evolution of cost functions over iterations of optimization in a sample calculation is shown in Fig. 1.

The calculation procedure for the case of both amplitude and phase modulations is similar, with the exception that Fourier series is adopted instead of the Bernstein polynomial, and we skip the details here. We regard the modulation waveform calculated above as a special example. Moreover, we believe that the choice of expansion basis is not unique and there exist many different types of waveforms that will satisfy the purpose. We anticipate that the deep learning algorithms will further improve this process of calculating appropriate waveforms.

II. TWO-ATOM DARK STATE

Ref. [1] provides a nice introduction of the two-atom dark state technique and how it helps to suppress the rotation error. Nevertheless, since the situation with our gate protocol is different from the typical π -gap- π framework of Ref. [1], we would like to offer more explanations on the underlying physical mechanism here.

When the two qubits start in states of $|01\rangle$ or $|10\rangle$, it only probes the ground-Rydberg transition in a straightforward manner. The Förster resonance structure will only be accessed when the initial state becomes $|00\rangle$, and this is exactly where the dark state driving mechanism may play an essential role. Main advantages include eliminating the rotation error and lowering the requirement on blockade strength.

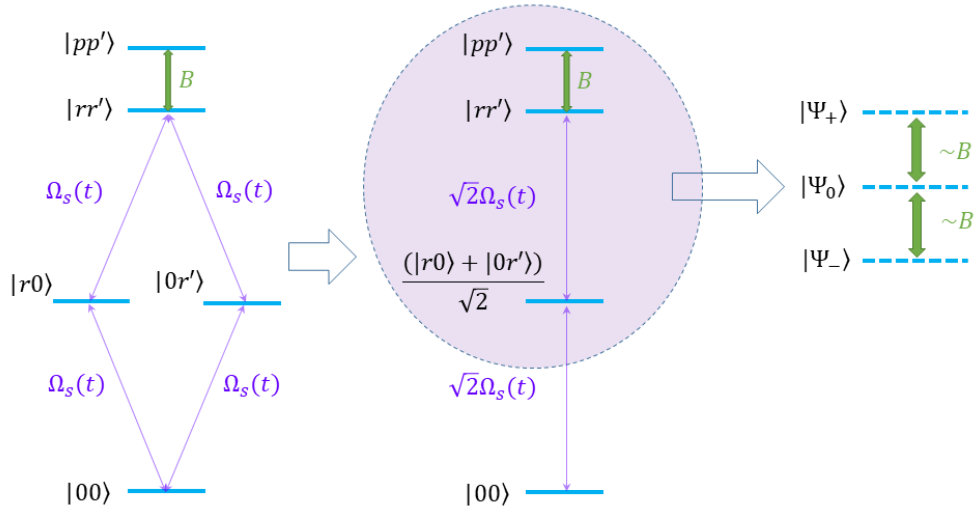


FIG. 2: Schematic of atomic levels of the dark state mechanism for the Rydberg phase gate under investigation, including the Förster resonance structure. The coupling between $|00\rangle$ and $(|r0\rangle + |0r'\rangle)/\sqrt{2}$ is given by Rabi frequency $\sqrt{2}\Omega_s(t)$ and detuning $\Delta(t)$.

At a first glance, the transition occurs between the launching state $|00\rangle$ and the target state $(|r0\rangle + |0r'\rangle)/\sqrt{2}$ (which will again be denoted as $|R\rangle$ to keep a succinct notation) under the idealized situation of perfect Rydberg blockade. Nevertheless, after taking the details of linkage structure into consideration as shown in Fig. 2, the situation of the target state becomes a consequence of the interactions between $|R\rangle$, $|rr'\rangle$ and $|pp'\rangle$. For simplicity we'd like to assume that the energy penalty term δ_p is zero. Therefore, the Hamiltonian for this system under the rotating wave approximation can be put down as the following matrix form:

$$\mathcal{H} = \hbar \begin{bmatrix} -\Delta & \frac{\sqrt{2}}{2}\Omega_s & 0 \\ \frac{\sqrt{2}}{2}\Omega_s^* & 0 & B \\ 0 & B^* & 0 \end{bmatrix} \quad (6)$$

For our case, it is customary to have $|\Omega_s| \ll |B|$ and $|\Delta| \ll |B|$ and therefore it makes sense to check the situation

with expansion up to 1st order in $|\Omega_s|/|B|$ and $|\Delta|/|B|$. The energy eigenvalues are:

$$\Delta_0 = -\Delta, \Delta_+ = |B|(1 + \frac{|\Omega_s|^2}{4|B|^2}), \Delta_- = -|B|(1 + \frac{|\Omega_s|^2}{4|B|^2}); \quad (7)$$

with the corresponding eigenstates listed below:

$$|\Psi_0\rangle = \cos \beta_2 \cos \beta_3 |R\rangle + \cos \beta_2 \sin \beta_3 |rr'\rangle - \sin \beta_2 |pp'\rangle, \quad (8a)$$

$$|\Psi_+\rangle = (\sin \beta_1 \sin \beta_2 \cos \beta_3 - \cos \beta_1 \sin \beta_2) |R\rangle + (\cos \beta_1 \cos \beta_3 + \sin \beta_1 \sin \beta_2 \sin \beta_3) |rr'\rangle + \sin \beta_1 \cos \beta_2 |pp'\rangle, \quad (8b)$$

$$|\Psi_-\rangle = (\cos \beta_1 \sin \beta_2 \cos \beta_3 + \sin \beta_1 \sin \beta_2) |R\rangle + (-\sin \beta_1 \cos \beta_3 + \cos \beta_1 \sin \beta_2 \sin \beta_3) |rr'\rangle + \cos \beta_1 \cos \beta_2 |pp'\rangle; \quad (8c)$$

while the angles of $\beta_1, \beta_2, \beta_3$ are defined as:

$$\tan \beta_1 = 1, \tan \beta_2 = -\frac{2\sqrt{2}|\Omega_s||B|}{\sqrt{2\Delta^2\Omega_s^2 + (\Delta^2 - 4B^2)^2}}, \tan \beta_3 = -\frac{\sqrt{2}\Omega_s\Delta}{\Delta^2 - 4|B|^2}; \quad (9)$$

where the expressions hold up to 1st order.

In particular, we want to take a closer look at $|\Psi_0\rangle$, which is the dark state coupling to $|00\rangle$. Up to 1st order, in fact $\sin \beta_3 \approx 0$. Therefore $|\Psi_0\rangle$ only practically contains components from $|R\rangle$ and $|pp'\rangle$. For the case of smoothly modulated pulse where $\Omega_s(t)$ starts and ends at zero value, $|\Psi_0\rangle$ coincides with $|R\rangle$ at the beginning and ending moments and thereby no significant amount population is left on the doubly excited Rydberg states after the gate protocol. Due to this effect and the fact that Δ_0 stays stable at the value of $-\Delta$ up to 1st order throughout the interaction process, the dark state mechanism eliminates the rotation error.

During this interaction process, adiabatic following plays an essential role to ensure the validity of dark state mechanism, and therefore it requires that the pulse waveform is sufficiently small and smooth to prohibit the influences of $|\Psi_+\rangle, |\Psi_-\rangle$. In other words, the condition may be stated as $|B| \cdot t_c \gg 1$ together with $(\Omega_{s0}/|B|)^2 \ll 1$ or simply $\Omega_{s0} \ll |B|$, where t_c is the characteristic gate time and Ω_{s0} is the mean amplitude of the waveform $\Omega_s(t)$. With respect to experimentally practical Rydberg blockade strength and laser parameters, this condition may be well satisfied.

III. PHASE MODULATION

The first errand right here aims at resolving the subtle details of handling frequency modulation in atom-light interaction. I'd like to begin with an EOM with respect to a rotating wave frame defined in a usual manner:

$$i\frac{d}{dt} \begin{bmatrix} C_0 \\ C_r \end{bmatrix} = \begin{bmatrix} 0 & \frac{1}{2}\Omega_s e^{i\frac{\theta}{2}\sin(\delta t)} \\ \frac{1}{2}\Omega_s e^{-i\frac{\theta}{2}\sin(\delta t)} & \Delta \end{bmatrix} \cdot \begin{bmatrix} C_0 \\ C_r \end{bmatrix}. \quad (10)$$

Afterwards, I will move one step further on top of the usual rotating phase, namely:

$$C_{r:\text{old}} = e^{-i\frac{\theta}{2}\sin(\delta t)} C_{r:\text{new}}; \quad (11)$$

which does not involve the phase of C_0 ; and this transforms the EOM for $C_{r:\text{new}}$ as:

$$i\frac{d}{dt} \begin{bmatrix} C_0 \\ C_r \end{bmatrix} = \begin{bmatrix} 0 & \frac{1}{2}\Omega_s \\ \frac{1}{2}\Omega_s & \Delta - \theta \cos(\delta t) \end{bmatrix} \cdot \begin{bmatrix} C_0 \\ C_r \end{bmatrix}. \quad (12)$$

In the above Eq. (12), intensity modulation (i.e. amplitude modulation) may also be incorporated as $\Omega_s \equiv \Omega_s(t)$ for real valued Ω_s . More generally, for:

$$i\frac{d}{dt} \begin{bmatrix} C_0 \\ C_r \end{bmatrix} = \begin{bmatrix} 0 & \frac{1}{2}\Omega_s e^{i\Theta(t)} \\ \frac{1}{2}\Omega_s e^{-i\Theta(t)} & \Delta \end{bmatrix} \cdot \begin{bmatrix} C_0 \\ C_r \end{bmatrix}; \quad (13)$$

I may define: $C_{r:\text{old}} = e^{-i\Theta(t)} C_{r:\text{new}}$; and then the EOM of Eq. (13) reduces to:

$$i\frac{d}{dt} \begin{bmatrix} C_0 \\ C_r \end{bmatrix} = \begin{bmatrix} 0 & \frac{1}{2}\Omega_s \\ \frac{1}{2}\Omega_s & \Delta - \frac{d}{dt}\Theta(t) \end{bmatrix} \cdot \begin{bmatrix} C_0 \\ C_r \end{bmatrix}. \quad (14)$$

Therefore, as long as $\frac{d}{dt}\Theta(t)$ is a linear combination of sinusoidal functions, so is $\Theta(t)$, which will be readily compatible with the experimental hardware of optical phase modulators working in the MHz–GHz range.

IV. PERFORMANCE UNDER REALISTIC IMPERFECTIONS

In this section, we further explore the performance of the gate, especially when it is subject to realistic imperfections commonly encountered in experimental investigations, including the influences of Rydberg states' spontaneous emissions, amplitude fluctuations in the laser pulse, and residual thermal motion of the cold atoms.

To incorporate spontaneous emissions of Rydberg states into the calculation, the decay rate of $|r\rangle, |r'\rangle$ is set as γ_r , while the decay rate of $|p\rangle$ and $|p'\rangle$ is set as γ_p . Moreover, to emulate technical noises such as random fluctuations on the amplitude, we set the Rabi frequency as $\Omega_s(t) + W \cdot \Omega_n$, where W takes random values in each MCWF trajectory uniformly distributed between 0 and 1. The corresponding numerical results for time evolution are shown in Fig. 3.

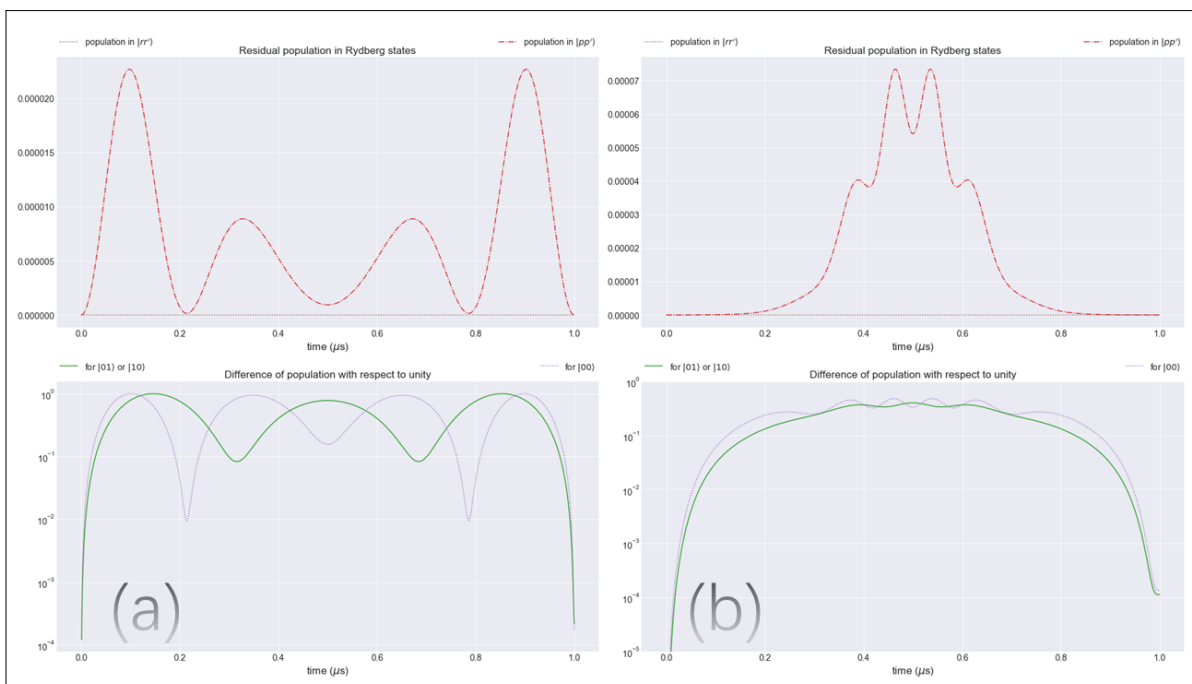


FIG. 3: More details about the performance of modulated waveforms, with the emphasis on the Rydberg population and spontaneous emission's effects. The simulation is for the time evolution of input state $|00\rangle$, averaged over 1 million MCWF trajectories. The settings are $\gamma_r = \gamma_p = \Omega_n = 2\pi \times 0.1\text{kHz}$. Here, parameter settings are kept the same as stated in main text, with the extra considerations for spontaneous emission from Rydberg levels and amplitude fluctuations. (a) Waveform with both amplitude and phase modulations defined as: $\Omega_s(t) = \Omega_0 + \Omega_1 \cos(2\pi t/T_g) + \Omega_2 \sin(\pi t/T_g)$, $\Delta(t) = \Delta_0 + \Delta_1 \cos(2\pi t/T_g) + \Delta_2 \sin(\pi t/T_g)$, corresponding to Fig. 2 of main text. The bottom figure shows that the population return with an error on the order of $\sim 10^{-4}$ after interaction. Apparently, the population of $|rr'\rangle$ remains negligible throughout the interaction. (b) Waveform with only amplitude modulation defined as: $\Omega_s(t) = \sum_{\nu=1}^4 \beta_\nu (b_{\nu,n}(t/T_g) + b_{n-\nu,n}(t/T_g))$, $\Delta(t) = \Delta_0 \equiv \text{constant}$, corresponding to Fig. 3 of main text. Again, we observe that the population of $|rr'\rangle$ remains negligible throughout the interaction.

The time evolution in Fig. 3 is computed via MCWF methods [2], and we sketch the procedure here. As stated in the main text, we let $|R\rangle = (|r0\rangle + |0r'\rangle)/\sqrt{2}$ denote the single-excitation Rydberg state connected with the ground state $|00\rangle$ via the optical driving field. The starting point is the set of equations of motions without considering the

spontaneous emissions, namely finite line-width of the Rydberg levels:

$$i \frac{d}{dt} \begin{bmatrix} C_0 \\ C_r \end{bmatrix} = \begin{bmatrix} 0 & \frac{1}{2}\Omega_s \\ \frac{1}{2}\Omega_s^* & \Delta \end{bmatrix} \cdot \begin{bmatrix} C_0 \\ C_r \end{bmatrix}; \quad i \frac{d}{dt} \begin{bmatrix} X_0 \\ X_R \\ X_{rr'} \\ X_{pp'} \end{bmatrix} = \begin{bmatrix} 0 & \frac{\sqrt{2}}{2}\Omega_s & 0 & 0 \\ \frac{\sqrt{2}}{2}\Omega_s^* & \Delta & \frac{\sqrt{2}}{2}\Omega_s & 0 \\ 0 & \frac{\sqrt{2}}{2}\Omega_s^* & 2\Delta & B \\ 0 & 0 & B & 2\Delta + \delta_p \end{bmatrix} \cdot \begin{bmatrix} X_0 \\ X_R \\ X_{rr'} \\ X_{pp'} \end{bmatrix}; \quad (15)$$

where C_0, C_r are for the dynamics associated with initial state $|10\rangle$ or $|01\rangle$ and $X_0, X_R, X_{rr'}, X_{pp'}$ are for the dynamics associated with $|00\rangle$. Then the decays may be built into the numerical evaluation by the means of quantum jumps. For a small time interval Δt , the probability of detecting spontaneous emission from $|r0\rangle$ or $|0r'\rangle$ is $\gamma_r \times \Delta t \times |C_r|^2$, the probability for $|R\rangle$ is $\gamma_r \times \Delta t \times |X_R|^2$, the probability for $|rr'\rangle$ is $2\gamma_r \times \Delta t \times |X_{rr'}|^2$, and the probability for $|pp'\rangle$ is $2\gamma_p \times \Delta t \times |X_{pp'}|^2$. If quantum jumps from the atomic spontaneous emissions do take place, then the atomic state is dragged into the specific eigenstates among the ground level, and we treat it effectively as the atomic population is lost outside of the system under consideration for practical numerical evaluation regarding gate fidelity. Note that one spontaneously emitted single-photon pulse will terminate the two-atom coherent dynamics since it is the two-qubit gate under study. If quantum jumps do not take place, the corresponding excited-state amplitudes shall be reduced. That is to say, $1 - \frac{\gamma_r}{2}\Delta t$ for C_r and X_R , $1 - \frac{\gamma_r}{\Delta}t$ for $X_{rr'}$, and $1 - \frac{\gamma_p}{\Delta}t$ for $X_{pp'}$.

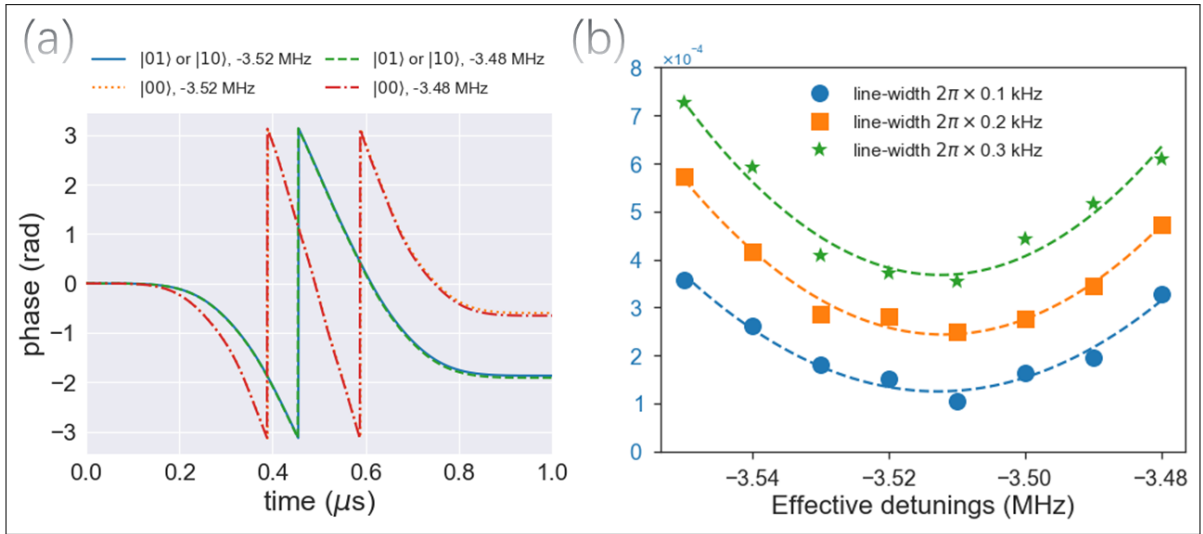


FIG. 4: Information about the performance of gate protocol under influence of detuning offsets, to account for the effects caused by residual thermal motion of the cold atom qubits. The calculations here correspond to the special case where both atoms travel at the same velocity. (a) Phase of the atomic wave function. The $\Delta_0 = -3.48$ MHz curve and $\Delta_0 = -3.52$ MHz curve almost overlap with each other. By the way, the population returns without significant loss. (b) Fidelities with different detuning offsets, each data point is averaged from 0.5 million MCWF trajectories, with settings as $\gamma_r = \gamma_p = \Omega_n = 2\pi \times 0.1$ kHz. Fitting to parabolic curve is also included.

Another intrinsic limitation is the residual thermal motion of the qubit atoms. As already been noticed during the experimental efforts with π -gap- π protocol, the atoms' kinematic motion in optical trap constitutes adverse influence to the gate fidelity. This becomes particularly annoying when the ground-Rydberg coupling is driven by the single-photon uv transition, even if the cold atom's thermal velocity is on the order of 1 cm/s – 10 cm/s. Approximately speaking, this detrimental effect is similar to the decoherence of ground-Rydberg Ramsey experiment on an atomic ensemble caused by the velocity distribution.

A typical example is shown in Fig. 4, where we carry out calculations with the same modulated amplitude but different effective detuning Δ_0 , in order to emulate the atom-light interaction process for atoms with non-zero velocity for the case of only amplitude modulation. It turns out, the off-resonant modulated driving technique is robust against this imperfection factor. This observation is also related to the fact that this gate protocol achieves necessary operations within a single continuous pulse while does not leave population in the Rydberg state during laser off time. Meanwhile, thanks to the dark state mechanism in the off-resonant modulated driving, even under the presence of detuning offsets, no significant population is left on the doubly excited Rydberg state after interaction.

V. SAMPLE CALCULATION OF A 250 NANO-SECOND GATE PROCESS

In this section, we discuss a sample calculation of a controlled-PHASE gate whose pulse duration is restricted to 250 ns. The purpose of a shorter pulse duration is to suppress the intrinsic error caused by the spontaneous emission from Rydberg states, which is the major theoretical limit for the off-resonant modulated driving gate protocol.

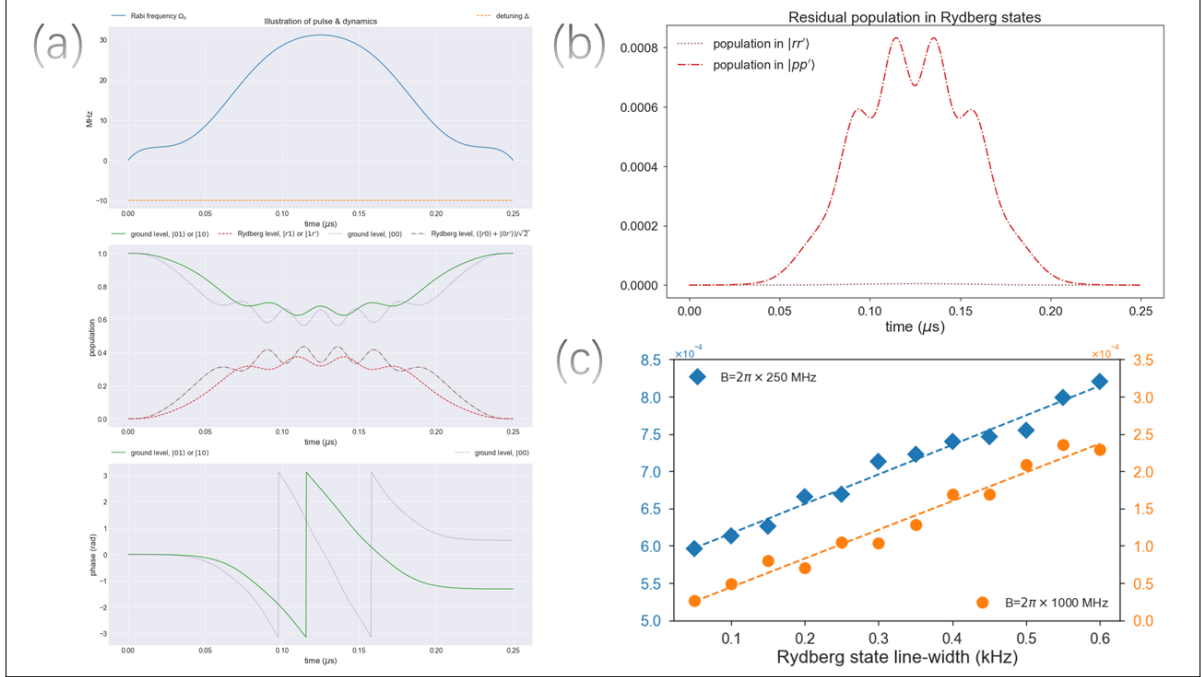


FIG. 5: Numerical results about the performance of a controlled-PHASE gate with time duration of 250 ns. (a) Details of the time evolution, without considering spontaneous emissions. The first graph shows the waveform, the second graph shows the population on different atomic states, while the last graph shows the phase accumulation of the atomic wave function during the atom-light interaction process. (b) Simulation for input state $|00\rangle$ with emphasis on population of Rydberg states during interaction. Similar to the $1 \mu\text{s}$ case, the population of $|rr'\rangle$ remains negligible throughout the interaction. The settings are $\gamma_r = \gamma_p = \Omega_n = 2\pi \times 0.1\text{kHz}$. (c) Gate fidelities under different conditions, where gate error is plotted against Rydberg decay rates. A local sing-qubit phase rotation is incorporated in the numerical simulation to transform controlled-PHASE gate into a standard C-Z gate. Due to the higher peak Rabi frequency values, it requires relatively stronger Förster resonance strength comparing with the case of $1 \mu\text{s}$ gate. Effects of spontaneous emissions and Rabi frequency amplitude fluctuations are considered, and each data point is from averaged evaluations over 0.5 million MCWF trajectories. The amplitude fluctuation is set as $\Omega_n = 2\pi \times 0.1\text{kHz}$.

Based upon the waveform calculation techniques presented in Section I, no fundamental difference exists between designing a $1 \mu\text{s}$ gate and 250 ns gate. However, from a practical point of view, laser power is not in unlimited supply for experimental apparatus. Therefore, we have designed a slightly different waveform with the intention of mildly suppressing the peak Rabi frequency on top of the previously discussed basic methods. Again, we have obtained a waveform for only amplitude modulation, which is constructed with respect to Bernstein polynomials. Here, the waveform is chosen as $\Omega_s(t) = \sum_{\nu=1}^8 \beta_\nu (b_{\nu,n}(t/T_g) + b_{n-\nu,n}(t/T_g))$, $\Delta(t) = \Delta_0 \equiv \text{constant}$ with $n = 16$. The relevant parameters include: $\beta_1 = 7.5308 \text{ MHz}$, $\beta_2 = 0.6184 \text{ MHz}$, $\beta_3 = 1.3992 \text{ MHz}$, $\beta_4 = 0.3316 \text{ MHz}$, $\beta_5 = 33.6 \text{ MHz}$, $\beta_6 = 38.4 \text{ MHz}$, $\beta_7 = 43.0396 \text{ MHz}$, $\beta_8 = 5.6926 \text{ MHz}$, $\Delta_0 = -9.96 \text{ MHz}$ and $T_g = 0.25 \mu\text{s}$. The numerical simulation of the gate performance is presented in Fig. 5, which demonstrates that shorter gate time duration helps to enhance gate fidelity, provided the Rydberg-Rydberg interaction strength is adequate.

Another interesting aspect is that, due to relatively larger atom-light detuning setting and shorter interaction time, in principle 250 ns gate becomes more robust against effects caused by residual thermal motion of the cold atom qubits, compared with $1 \mu\text{s}$ gate. However, on the other hand, at this moment it seems that the gate time cannot be reduced to an arbitrarily small time interval yet. The reason comes from the reality that Rydberg-Rydberg interaction

strength may not be experimentally enhanced unlimitedly, at a finite atom-atom distance.

VI. WHEN RABI FREQUENCIES ARE NOT BALANCED DUE TO IMPERFECTIONS

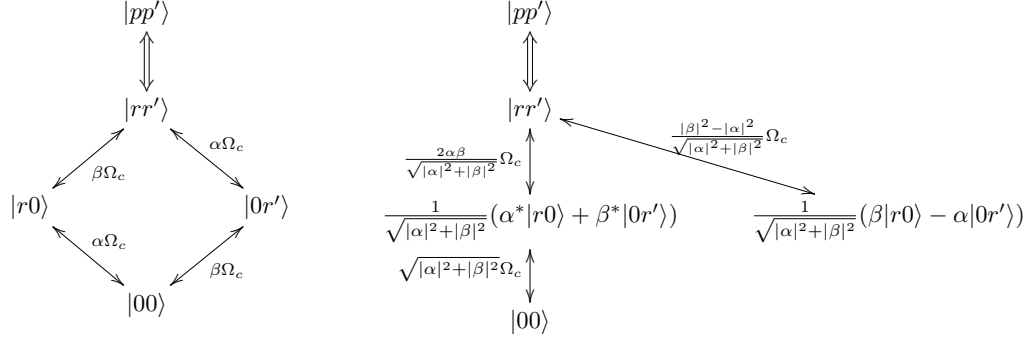


FIG. 6: Transition linkage pattern for the ladder type linkage configuration under consideration, with asymmetric optical driving on two qubit atoms. Morris-Shore transform is employed to show the reduced transition structure and the associated effective Rabi frequencies are also marked. The uncoupled idle state for $|00\rangle$'s ground-Rydberg transition to a singly Rydberg excited state is $(|\alpha|^2 + |\beta|^2)^{-1/2}(\beta|r0\rangle - \alpha|0r'\rangle)$; however its transition strength to $|rr'\rangle$ does not vanish and shall be included in a serious calculation.

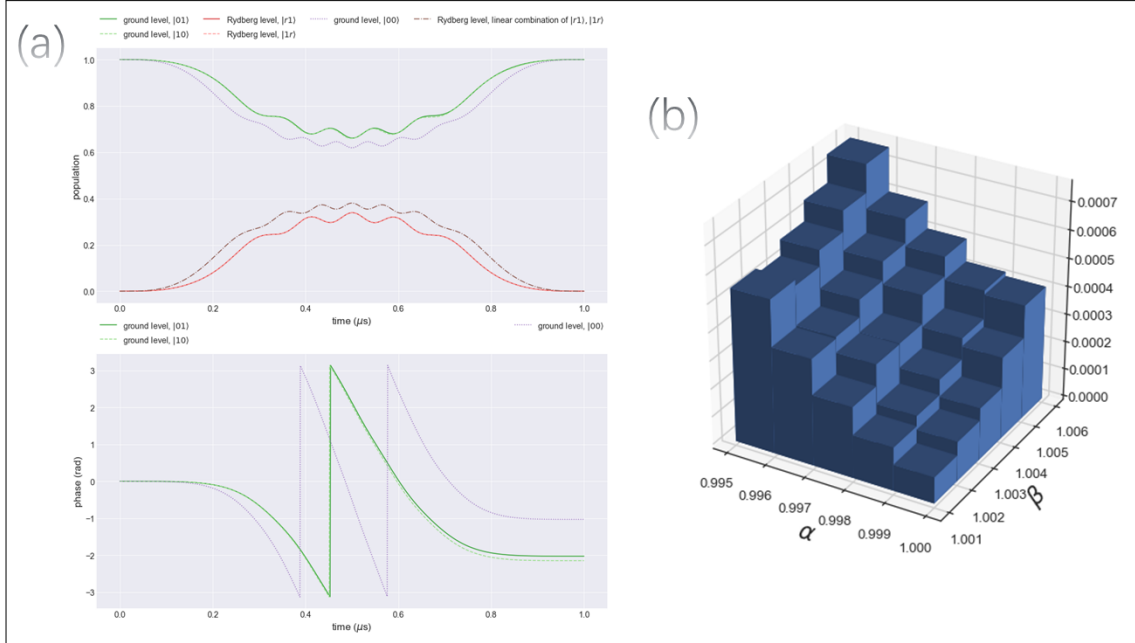


FIG. 7: Information about the performance of gate protocol under the influence of asymmetric driving. (a) Details of the time evolution, without considering spontaneous emissions. The first graph shows the population on different atomic states, while the second graph shows the phase accumulation of the atomic wave function during the atom-light interaction process. (b) Simulation of gate errors under asymmetric driving.

Generally, we only consider it as an idealization to establish a perfect equivalence between the Rabi frequencies

at the sites of the two atomic qubits. Under realistic experimental conditions, the ratio may be set close to 1 but with some minor deviations due to systematic uncertainties, and this ratio may vary shot-to-shot. Therefore, it is reasonable to investigate the gate protocol's performance under such circumstances and estimate its robustness.

We assume that the ideal Rabi frequency is Ω_c , and the actual Rabi frequencies due to asymmetric driving are $\alpha\Omega_c, \beta\Omega_c$ at the two qubit atoms respectively. First of all, the time evolutions of initial state $|01\rangle$ and $|10\rangle$ become different due to asymmetry. Meanwhile, the linkage structure and level configurations involved in the time evolution for initial state $|00\rangle$ are more complicated than the case of perfect symmetric driving, whose details are shown in Fig. 6. Those extra complexities all need to be included in the calculations of the dynamics of the system under study.

Then we carry out numerical simulations to estimate the relevant effects, where a typical sample result is shown in Fig. 7. For Fig. 7(a), we choose the same waveform of only amplitude modulation as the main text and Section IV. In order to clearly demonstrate the influence of the asymmetric driving, the parameters are set as $\alpha = 0.995, \beta = 1.005$ which constitutes a significant deviation from the ideal configuration. For Fig. 7(b), we examine the gate fidelities under different extents of asymmetry and plot the gate error as a function of α, β . Effects of spontaneous emissions and Rabi frequency amplitude fluctuations are considered, and each data entry is from averaged evaluations over 0.2 million MCWF trajectories. The settings are $\gamma_r = \gamma_p = \Omega_n = 2\pi \times 0.1\text{kHz}$.

-
- [1] D. Petrosyan, F. Motzoi, M. Saffman, and K. Mølmer, Phys. Rev. A **96**, 042306 (2017).
 [2] J. Dalibard, Y. Castin, and K. Mølmer, Phys. Rev. Lett. **68**, 580 (1992).